PRESSURE MEASUREMENTS IN A WIRE-WRAPPED 61-PIN HEXAGONAL FUEL BUNDLE

A Thesis

by

PHILIP G. JONES

Submitted to the Office of Graduate and Professional Studies of
Texas A&M University
in partial fulfillment of the requirements for the degree of

MASTER OF SCIENCE

Chair of Committee,	Yassin Hassan
Committee Members,	N.K. Anand
	Rodolfo Vaghetto
Head of Department,	Andreas A. Polycarpou

December 2017

Major Subject: Mechanical Engineering

ABSTRACT

The sodium fast reactor is a type of liquid metal fast breeder nuclear reactor. Fast reactors offer a number of benefits over conventional thermal reactors such as, a more abundant source of fuel, and are inherent increases in safety. Fast reactor technology was actively pursued in the 60's and 70's but interest in the nuclear industry slowed shortly thereafter as did interest in fast reactor technology. The increase in demand for cleaner safer energy has resulted in an increase in research into liquid metal fast reactors.

In the interest of safety and improved efficiency, significant research efforts, both in the past and the present, have investigated coolant flow properties in LWR fuel bundles. These bundles pack the fuel pins in a square array and utilize spacer grids at various points along the bundle's length. Contrast to SFR fuel bundles that arrange the fuel pins in a triangular array that are spaced evenly with a wire spacer that is wrapped helically around the fuel rod. There exists extensive literature and experimental data which characterize the flow in this complex geometrical configuration, but not all combinations of parameters have been investigated, and more modern instrumentation could lead to more accurate data.

This work has produced pressure measurements at two axial locations for a wide range of Reynolds number. High accuracy instrumentation was used and the uncertainty in the measurements has been quantified. Azimuthal differential measurements have also been produced at two axial locations.

.

CONTRIBUTORS AND FUNDING SOURCES

Contributors

This work was supported by a thesis committee consisting of my advisor Professor Yassin Hassan of the Department of Nuclear Engineering, Professor N.K. Anand of the Department of Mechanical Engineering, and Professor Rodolfo Vaghetto of the department of Nuclear Engineering.

The facility was constructed and the experiments performed with the help of Dr. Thien Nguyen, Nolan Goth, Mason Childs, Nico Quintanar, and Will Headley.

All other work conducted for this thesis was completed by the student independently.

Funding Sources

This experimental facility described in this article was design and constructed under a project by the Department of Energy (Award Number DE-NE0008321). Part of the experimental data produced during this activity is sponsored and funded by the Nuclear Energy University Program (Project Number 17-12502)

TABLE OF CONTENTS

LIST OF FIGURES

Page

LIST OF TABLES

Page

1. INTRODUCTION

The thermal-hydraulic response of flows in various configurations of rod bundles have been extensively studied in the past. Rod bundles are used in a wide variety of heat transfer and flow applications. They are also used in nuclear reactors, the most common being the fuel is formed into a cylindrical shape and the thermal energy is transferred to a fluid to be used for some other process downstream. The exact response of flow characteristics is highly dependent on the geometrical configuration the rod bundle is arranged in. Extensive research has been conducted in square lattice bundles, particularly related to light water reactors with spacer grids. Fast reactor designs use triangular lattice arrays. Different types of spacers have been investigated, and one design uses a wire spacer wrapped around each rod where the rods are in contact with the spacer.

The first efforts to investigate triangular lattice wire-wrapped bundles began as early as the 1970's. Multiple experiments were carried out over the next couple decades, but eventually interest slowed. Recently interest has increased and has resulted in the need for more data. Most data available is primarily in the transition and turbulent regimes as they are of most importance during normal operation. With a greater emphasis on safety and preparedness with regards to nuclear accidents, datasets are required to be more accurate and expansive. All flow regimes need to be investigated and higher accuracy instrumentation results in less uncertainty in the data. One of the most important parameters through fuel elements is the pressure drop caused by the array of rods, and is of great concern to designers with regards to design and

optimization. The pressure drop through the bundle is highly useful for the assessment and development of correlations used to predict pressure losses, and is also useful for the validation of Computational Fluid Dynamics models

2. OBJECTIVE

The primary objective is to characterize the pressure response in a wire-wrapped hexagonal fuel bundle and produce a highly accurate extensive dataset. Past experiments focused primarily on the pressure response in the turbulent flow regime, because most if not all reactor designs benefit from the higher heat transfer rates possible in highly turbulent forced convection. As designs progress past the prototype stage, evaluation of safety under all potential conditions becomes more important, and all flow conditions must be investigated. This objective will be achieved by the following:

- Generate highly accurate data, reduce uncertainty.
- Measure axial pressure drop.
- Measure azimuthal pressure drop.

Cover all flow regimes, laminar through turbulent.

- Evaluate the uncertainty in the measurements.
- Comparison of data to correlation predictions.
- Produce bundle friction factor as a function of Reynolds number.

3. LITERATURE REVIEW

Rod bundles are used in a variety of different engineering applications, especially as a means of heat transfer. Typically, a fluid flows on the exterior, the interior, or both as a means to convect the thermal energy from one place to another. In nuclear power reactors, the nuclear the nuclear fuel is formed into a cylindrical shape and clad inside a cylindrical shroud. As the fluid moves past this arrangement of cylinders, the fuel rods impede the flow which results in a pressure drop. This drop in pressure is of significant importance in the design and optimization of heat transfer applications. For this reason, the exact pressure response of a particular geometry needs to be quantified, and methods need to be in place to predict the outcome of geometric and fluid variables.

In the case of vertical axial flow with the tubes parallel to the flow, the total static pressure drop consists of a gravitational term and a frictional term. The gravitational is simply a function of the change in elevation and the density of the fluid, but the frictional term is a function of the geometry and the fluid properties. This frictional term can be solved for analytically in the case of very simple problems, such as infinite plates and smooth pipe flow, but for complex situations, the frictional losses are determined empirically and experimentally.

In the case of sodium cooled fast reactors, fuel pins are arranged in a triangular lattice. The pressure drop in bare rods has been quantified in the past, which is primarily a function of the pitch or distance between adjacent rods. Current designs suggest using a helically wrapped wire around the rods to be used as a spacer and as a means to

increase mixing between subchannels and subsequently increase the overall heat transfer.

This spacer induces a swirl pattern of the fluid through the rods and increases the complexity in determining the pressure response in the bundle. Multiple experimental data sets and correlations have been created and found that the frictional pressure drop is a function of the pitch, pitch to diameter ratio, number of pins, diameter of the pins, diameter of the wires, and the distance from the last pin to the edge of the duct. A variety of combinations has been investigated in multiple flow regimes, but not all combinations have been.

Cheng Tondreas and Nguyen conducted an evaluation of existing correlations and compared the predicted values of each to the existing experimental data sets [1]. They presented a fairly comprehensive list of data sets available, although there have been a few more recent experiments conducted. A small portion of the data sets were generated with rod bundles that have a larger wall gap size compared to others. The bundle in this work was fabricated entirely of plastics where maintaining tight tolerances is difficult. This has resultd in this bundle having the largest wall gap.

Novendstern in 1972 applied a semi-empirical model to about 40 experiments available at that time [2]. This correlation assumes the flow is split evenly through all subchannels and evaluates the friction factor based on the central subchannel with an empirical correction factor that accounts for the wire effects. This correction factor is multiplied by the friction factor for the equivalent Re number in a smooth pipe then

multiplied by the equivalent diameter ratio to the bundle to approximate the bundle averaged friction factor.

Rehme in 1973 took a different approach where he derived an effective velocity to approximate the frictional losses caused by the swirl of the flow around the rod [3]. An empirical formula was then calibrated using the modified velocity against Rehme's own data set. This correlation is still widely used, but offers no prediction in the laminar flow regime.

Engal et al. in 1979 developed a model for blanket assemblies with low P/D ~ 1.08 and H/D ~ 8; it is not suitable for other bundle geometries [4]. Engal was the first to propose a correlation for the laminar regime, but the limited data set used renders it unable to accurately predict the friction factor for other geometries. To predict the pressure response in the transition region, an intermittency factor was introduced, which is a weighting function between the predicted laminar constant and the predicted turbulent constant.

Cheng and Tondreas in 1986 were the first to propose a subchannel approach in order to evaluate the bundle friction factor [5]. It was postulated that the frictional losses in the interior subchannels are different in nature that in the edge and corner subchannels. In essence the interior region can be modeled by skin friction and drag effects caused by the wire whereas the edge and corner subchannels exclude the wire drag effects because the flow is nearly parallel with the wire. This correlation also includes an empirical model based on bundle geometry that predicts the transition points, from laminar to transition and from transition to fully turbulent. An intermittency factor

similar in form to the one proposed by Engal et al. was also utilized, and in 2013 was modified with a slight change to one of the exponents [6].

Baxi and Dalle Donne in 1981 combined the Engal laminar constant model with the Novendstern model for the turbulent regime [7]. Also included was a way to account for the coolant temperature profile. One limitation is that it assumes fixed transition points that are not a function of geometry.

Chen et al. evaluated a number of correlations presented by Kirillov that developed by Russian scientists [8]. Chen combined the best parts of them and is referred in their text as the Kirillov model.

The early correlations were mostly empirical and somewhat limited in applicability, at least as far as flow regimes. They later included all regimes and incorporated physical hydrodynamic models, but pursuit in developing these correlations further has stalled. This is partly due to a much greater emphasis on CFD in research. As SFR designs progress beyond the initial development stage, the number of simulations and analysis required for licensing could see the industry relying more on these correlations.

4. EXPERIMENTAL SETUP

4.1. Facility Description

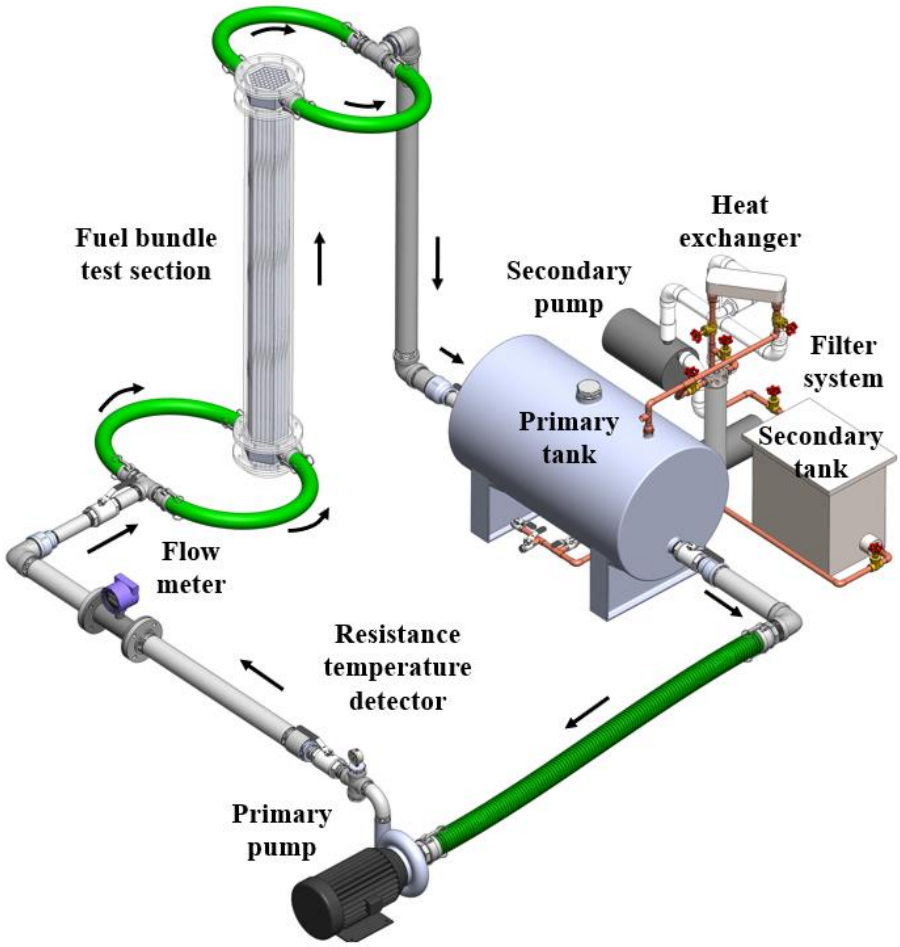

Figure 1. Experimental facility overview.

This project was conducted in conjunction with outside organizations to produce the data necessary to aid in the validation of a CFD model. This facility conducted isothermal experiments while a sister facility conducted heated experiments. In order for

theses sister facilities to be of use, care must be taken that they have the same geometrical parameters notably, the number of pins, the pitch to diameter ratio, and the wire pitch lead length to pin diameter ratio. These values are shown in Table 1 and depicted in Figure 3. To produce the data required, supplementary components had to be acquired and constructed.

The experimental facility consists of a primary and a secondary flow loop. The following components make up the primary loop.

- Test fuel bundle of 61 pins in a triangular lattice housed in a hexagonal duct.
- Primary tank that contains the working fluid as a surge volume.
- Primary centrifugal pump and corresponding VFD to control the volumetric flow-rate.
- Turbine flow meter to evaluate the volumetric flow-rate.
- Resistance temperature detector (RTD).
- Pressure transducers to quantify the gauge and differential pressure at various locations.

The secondary loop was added to maintain the fluid temperature and provide a means to filter the fluid. This was accomplished with a heat exchanger and chilled water supply. A 25 micron filter is used to remove seed particles from the fluid when necessary. Temperature control is required when velocity measurements are conducted in conjunction with the pressure measurements. The technique used to measure the velocity in the subchannels is the matched index of refraction (MIR) technique where the refractive index of the fluid is matched to the refractive index of the solid materials.

Because refractive index is temperature dependent, a constant temperature must be maintained within a small margin.

Two working fluids were used, DI water and p-Cymene. The volatile nature of p-Cymene necessitated chemically resistant materials be utilized throughout the facility such as, stainless steel, Viton seals, and cross-linked polyethylene. Care was taken to isolate the test section from the vibrations induced by the primary pump by erecting the test section on a structure not rigidly connected to the stainless-steel piping. Flexible tubing joins the inlet and outlet plenum to the stainless steel piping.

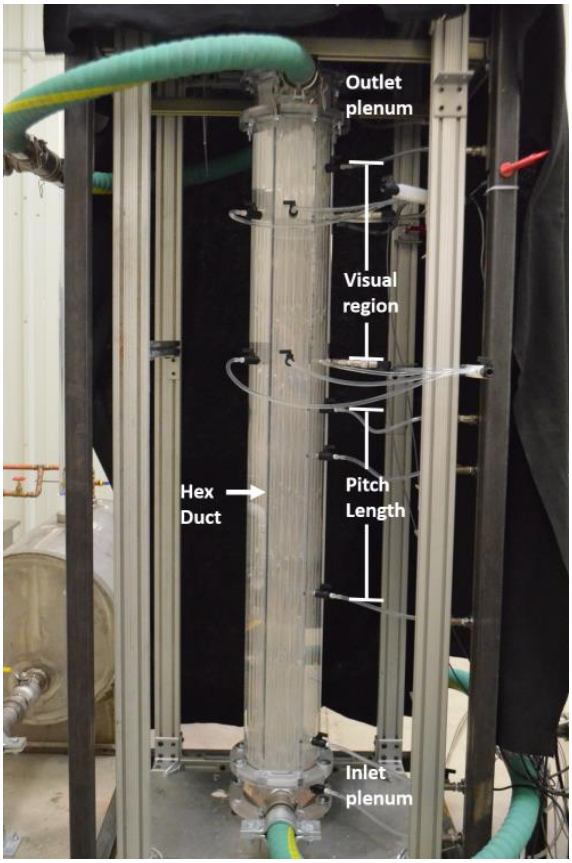

Figure 2. Test section

The test section consists of a flow visualization region, an inlet plenum, and an outlet plenum, shown in Figure 2. Flow enters the inlet plenum via two flexible hoses and directs the fluid upward into the flow visualization region. The inlet plenum also houses a grid plate which fixes the pins in the bundle geometry. The outlet plenum also contains a grid plate to fix the pins, and also serves the purpose of directing the flow out of the test section via two flexible hoses. The geometric parameters of the test section are listed in Table 1 and depicted in Figure 3.

Table 1. Test section dimensions.

Symbol	Description	Value (m)
FTF	Flat-to-flat distance	0.154
P	Rod Pitch	1.189×10^{-2}
D_{pin}	Rod diameter	1.189×10^{-2}
D_{wire}	Wire diameter	1.189×10^{-2}
W	Edge pitch	1.189×10^{-2}
H	Wire pitch	0.476
CTC	Corner-to-corner distance	0.178
Gap_{wall}	Wall gap size	6.71×10^{-4}
H/D	Helical pitch to pin diameter ratio	30
P/D	Rod pitch to pin diameter ratio	1.189
L	Bundle total length	1.857
L_c	Bundle length in central section	1.667

The Flow visualization region houses 61 pins in a triangular lattice arrangement contained within a hexagonal duct. Each pin is wrapped helically by a single wire

spacer. This spacer contacts the adjacent pins, and in the case of exterior pins, the duct wall. This ensures the pins are tightly packed and immobilized in the duct.

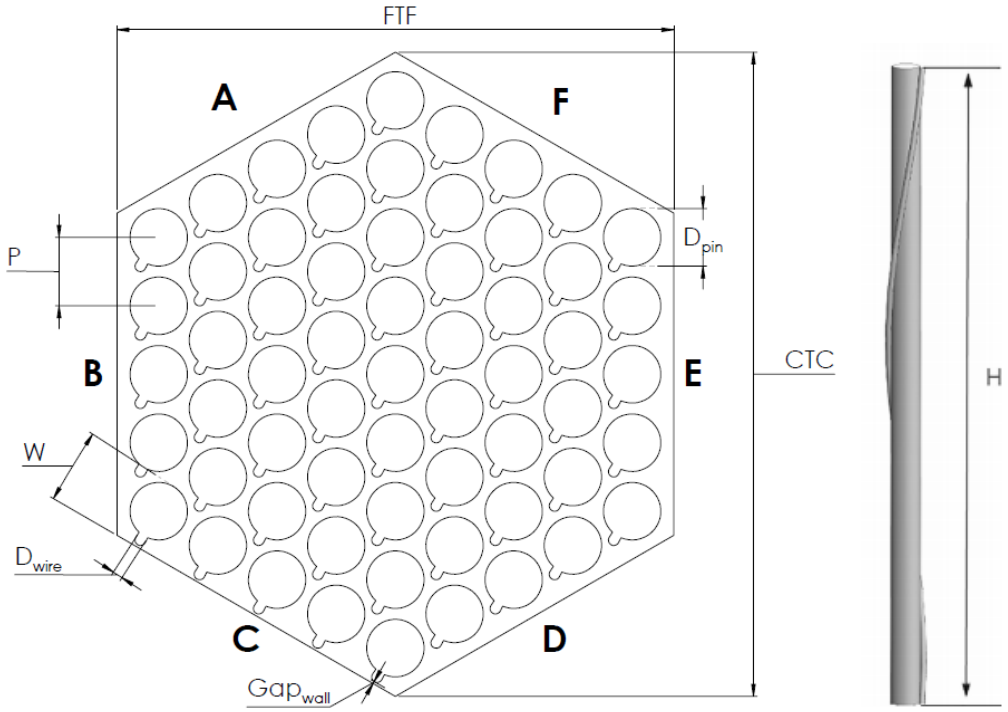

Figure 3. Cross section of 61-Pin hexagonal fuel bundle and geometry.

4.1.1. Instrumentation

Pressure Hardware

The pressure transducer hardware installed in the experimental facility is summarized in Table 2. The accuracy of each transducer is relative to its full scale (FS) reading. Nine pressure transducers are installed at different axial locations (denoted as pressure taps PT#0-8) also listed in Table 2. All pressure taps are located at the center of

face F. They were initially attached to the wall with PVT tubes, then later installed directly on the duct's wall. PT#0 is located at the inlet plenum to monitor and control pressure of the test section inlet (maximum operating pressure). The total pressure drop through the entire test section is measured by the difference in pressure measured by PT#0 (inlet tap) and PT#8 (outlet tap). Pressure transducers PT#1-7 are used to record the pressure at seven axial locations along the test section, including the development region. These pressure taps allow for the determination of the bundle averaged friction factor.

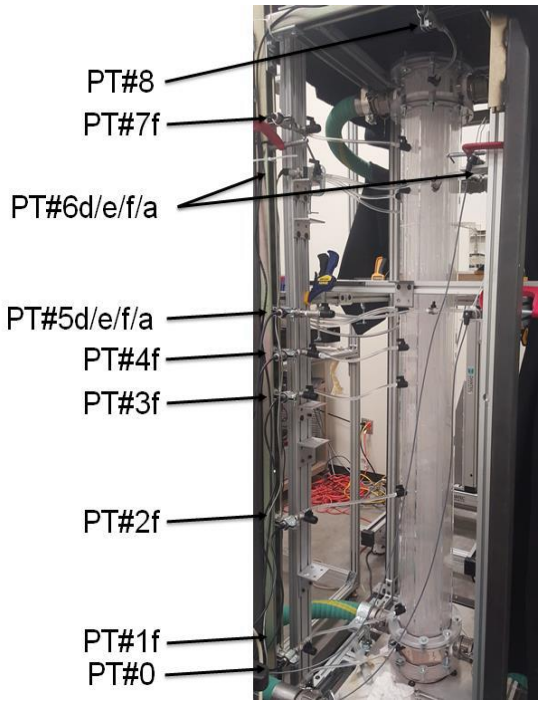

Figure 4. Pressure tap locations

It was determined that the use of the gauge pressure transducers to estimate the friction factor results in unsatisfactory uncertainty. For this reason, an additional high accuracy differential transducer was installed between PT5 and PT7. This location is in the fully developed region and is also used for flow visualization. The wire clock angle impacts the pressure in the wall subchannel and is the reason the location between PT5 and PT7 was chosen; they are one full wire pitch apart with the same wire angle.

Two axial locations, PT5 and PT6, also had pressure taps on faces A, D, and E. These pressure taps allow for the measurement of the pressure difference azimuthally. A high accuracy differential pressure transducer is connected to these taps via two manifolds. Actuation of valves on theses manifolds control which two locations the differential transducer measures.

Table 2. Pressure transducer accuracy

PT #	Axial Location (Wire Pitch)	Full Scale (Pa)	Accuracy (%Full Scale)
0	Inlet	206843	< 4.0
1	0.16	206843	< 4.0
2	1	206843	< 0.1
3	1.75	206843	< 0.1
4	2	206843	< 0.1
5	2.25	103421	< 0.1
5_d/e/f/a	2.25	2488	< 4.3
6	3	206843	< 0.1
6_d/e/f/a	3	2488	< 0.1
7	3.25	103421	< 0.1
8	Exit	103421	< 1.0
5-7DP	2.25-3.25	6895	< 1.0
2-6DP	1.00-3.00	34474	<1.0

Temperature

An RDF Corporation resistance temperature device (RTD) is utilized to measure and record the temperature of the fluid during the experiments. The accuracy of the device is ±0.3˚C at 0˚C with an operating range of -196 ˚C to 480˚C. The RTD is located near the primary pump outlet.

Flow Meter

A Sponsler in-line precision turbine flowmeter (SP3-MB-PHL-D-4X) is installed near the test section inlet and is utilized to measure the volumetric flow rate of the working fluid. The uncertainty of the flowmeter analog output is 0.025% of full scale at 20 °C. The full scale reading is 2271 l/min. A Sponsler IT400 totalizer records the analog output from the flowmeter with a digital uncertainty of ±3.8 l/min.

The construction of the total facility progressed from initial construction, shakedown testing with de-ionized water, then testing with p-Cymene. The flow meter was initially procured with a calibration for de-ionized water. p-Cymene has a density and dynamic viscosity roughly 80% that of water [9]. For a turbine meter, the calibration parameter, referred to as the K-factor, is a function of both density and viscosity and generally can only be determined empirically. Metering p-Cymene with the K-factor calibrated for water resulted in the measured volumetric flow rate being undervalued. An in house calibration of the flow meter was conducted.

Two approaches to calibrate the flow meter were attempted. The first was simply flowing the p-Cymene into a large reservoir, marking graduated lines of the fluid added in a finite interval, and measuring the volume added to the reservoir per unit time. This

proved to be an accurate method for low flow rates, but at higher flow rates the fluid churned chaotically and proved difficult to accurately determine the amount of fluid added.

The second approach was to calibrate against a different type of flow meter. Differential pressure flow meters are dependent on density of the fluid only, such as orifice plates and pitot tubes. A loop that bypassed the test section was constructed and a self-averaging pitot tube was installed. This allowed for the turbine flow meter to be calibrated against the pitot tube flow meter.

The pitot tube has an accuracy of 0.1% of indicated rate. The uncertainty of the flow is a function of the pitot tube's accuracy as well as the accuracy of the instrument used to measure the differential pressure. Volumetric flow rate is determined by the pressure drop from the pitot tube. To minimize uncertainty in the volumetric flow rate, three different high accuracy differential transducers with full scale pressures of 0.36 psi, 1.0 psi, and 5.0 psi were used. The measured pressure from the smallest full scale transducer that was not off scale was used to calculate the flow rate. This approach was justified as the friction factor results for p-Cymene as a function of Reynolds number were in agreement with the water results.

Data Acquisition

Pressure transducers, RTD, and flow meter are connected to a National Instrument data acquisition system and interfaced to a laptop computer using LabVIEW. Pressure, temperature, and flow rate data is continuously recorded during the tests.

4.2. Experimental Procedure

Experimental tests were conducted in order to generate a collection of pressure drop data. This data was used to evaluate the bundle averaged friction factor over a wide range of Reynolds number in the laminar, laminar-to-transition, transition-to-turbulent, and turbulent flow regimes. In preparation of the tests, written procedures were followed to verify the test equipment and instrumentation was functioning properly. Prior to the test, the output from the pressure hardware was compared to two known values, static and roughly 50 GPM. Once the hardware was verified, an experimental test could continue and consisted of the following steps:

1. The pump speed was adjusted using the primary VFD until the desired volumetric flow rate was achieved. Before data was collected, the pump speed was maintained for a sufficiently long period of time to guarantee that steady flow conditions were achieved in the loop and test section;
2. The pump operated continually while three consecutive sets of 10-second pressure measurements were recorded through the DAQ system. Flow meter output was also logged digitally during this step.

3. The procedure was repeated from step one at all volumetric flow rates of interest. Additionally, the static or no flow measurement was sampled before the flow tests were conducted as well as after the tests were conducted.

As stated in the previous section, the working fluid was p-Cymene to allow use of the matched index of refraction flow visualization technique. Temperature of the primary fluid was monitored and logged throughout all tests. During tests that coincided with flow visualization tests, the temperature was maintained at ambient conditions to stabilize the index of refraction of the fluid. This was accomplished by transferring the heat to the secondary flow loop, thermally coupled by the heat exchanger. During tests that did not coincide with visualization measurements, the temperature was logged instead of controlled. This allowed for temperature dependent estimations of Reynolds number and friction factor.

5. DATA EVALUATION

5.1. Reynolds Estimation

The bundle average Reynolds number is calculated using Eq. 1 where V is the fluid velocity, D_h is the hydraulic diameter, and v is the temperature dependent kinematic viscosity.

$$Re = \frac{V D_h}{\nu} \tag{1}$$

The fluid velocity is determined by dividing the arithmetic average of the volumetric flow rate indicated by the flow meter, and the bundle flow area.

The hydraulic diameter is calculated from Eq. 2, where A represents the flow area, and P_{wet} represent the wetted perimeter of an azimuthal cross section of the bundle.

$$D_h = \frac{4A}{P_{wet}} \tag{2}$$

Formulations of theses geometric calculations are shown in appendix A, and consist of the duct wall, pin diameter, and elliptical projection of the inclined wire spacer.

Thermal properties of p-Cymene were taken from [9], but given the limited temperature range used in testing, only two data points exist for these experiments. Additional verification of the fluid properties, mainly density and viscosity, were performed using a rotational viscometer. The relationship was determined to be nearly linear in the range of 20-25 °C, and linear interpolation of the referenced source for p-Cymene thermal properties is acceptable.

5.2. Experimental Friction Factor

The primary parameter to evaluate the bundle against other experimental bundles is the bundle averaged friction factor. The friction factor is evaluated from the pressure drop over one wire pitch, the geometry of the bundle, and the fluid velocity through the bundle as represented by Eq. (3).

$$f = \Delta P \left(\frac{D_h}{L}\right)\left(\frac{2}{\rho V^2}\right) \tag{3}$$

Most of the data generated was measured between PT5 and PT7, as they are in the fully developed region and coincide with the visualization region of interest. Other data points were derived from the pressure drop between PT4 and PT6, which are also one wire spacer pitch apart, and PT2 and PT6 which are two pitches apart. Each pair of tap locations have the wire at the same position relative to the wall. Taking the pressure drop at from two locations that are not at the same wire clock angle introduces error in the experimental friction factor, because there exists a pressure spike on the front side of the wire and a pressure depression on the back side. The measured pressure drop used is the average of the three repeated trials at a given flow rate of interest.

5.3. Uncertainty Analysis

The uncertainty of the fluid velocity and pressure measurements were propagated. The primary contributions to the velocity uncertainty were the repeatability of the turbine flow meter, and the in-house calibration performed with the pitot tube. The

standard deviation of the fluid velocity is calculated from the standard deviation of the volumetric flow rate, $\sigma_{Q.}$

$$\sigma_V = \frac{\sigma_Q}{A} \tag{4}$$

The volumetric flow rate uncertainty is derived from the standard deviation of the flow meter and the associated calibration, $\sigma_{Flow\ Meter}$ and $\sigma_{Calibration.}$

$$\sigma_Q = \sqrt{\sigma_{Calibration}^2 + \sigma_{Flow\ Meter}^2} \tag{5}$$

The calibration uncertainty consisted of the accuracy of the pitot tube measured volumetric flow rate, $\sigma_{Q,Pitot,.}$and the accuracy of the magnetic coil that measures the frequency of the turbine in the flow meter, σ_{Freq}.

$$\sigma_{Calibration} = \sqrt{\sigma_{Q\ Pitot}^2 + \sigma_{Freq}^2} \tag{6}$$

The standard deviation of the pitot tube volumetric flow rate is a combination of the rated accuracy of the pitot tube and the pressure transducer accuracy.

$$\sigma_{Q\ Pitot} = \sqrt{Pitotaccuracy^2 + PTaccuracy^2} \tag{7}$$

To account for the uncertainty in the Reynolds number, the uncertainty in the fluid velocity through the bundle was propagated as shown below.

$$\sigma_{Re} = \frac{\sigma_V D_h}{\nu} \tag{8}$$

The pressure drop across the pitot tube increases as the volumetric flow rate. In order to minimize the uncertainty at lower flow rates, the lowest full-scale differential pressure transducer was utilized as allowed given the drop in pressure generated by the pitot tube. Because the different transducers have a different rated accuracy, this resulted

in the standard deviation of the flow meter calibration being a function of volumetric flow rate. To account for this, a K-Factor table was generated as a function of flow meter turbine frequency where each K-Factor entry had an associated standard deviation. This uncertainty was then combined with the accuracy of the turbine meter as shown in Eq. 6 and subsequently fluid velocity and Reynolds number.

The standard deviation of the experimental friction factor comprises of the uncertainty in the pressure measurement and the fluid velocity.

$$\sigma_f = f\sqrt{\left(\frac{\sigma_{\Delta P}}{\Delta P}\right)^2 + \left(\frac{\sigma_V}{V}\right)^2} \tag{9}$$

The pressure measurement uncertainty accounts for the hardware accuracy and the variation in the repeated measurement. A static or no flow measurement was sampled to quantify any erroneous readings caused by the physical orientation of the transducer. Below shows the standard deviation of the no flow measurement.

$$\sigma_{NoFlow} = \sqrt{\left(\frac{PTaccuracy}{2}\right)^2} \tag{10}$$

The standard deviation of a pressure measurement for a given flow rate including the variation of the repeated measurements is calculated as shown below.

$$\sigma_{xFlow} = \sqrt{\left(\frac{PTaccuracy}{2}\right)^2 + \sigma_{Means}^2} \tag{11}$$

The experimental friction factor was generated either from a differential pressure measured directly by a differential transducer, or by the difference between two gauge transducers. For the case of two gauge transducers, the differential pressure uncertainty

is calculated as shown in the equation below, where the subscripts indicate two arbitrary axial pressure tap locations.

$$\sigma_{\Delta P} = \sqrt{\sigma_{xFlow,i}^2 + \sigma_{xFlow,j}^2} \tag{12}$$

When a differential transducer was used to measure the differential pressure directly, the standard deviation in the differential pressure measurement was simply,

$$\sigma_{\Delta P} = \sigma_{xFlow} \tag{13}$$

6. RESULTS

6.1. Reference Correlations

The pressure drop correlations outlined in section 3 were developed based on several existing experimental data to estimate friction factor. The friction factor of a bundle is influenced by a wide range of parameters, such as number of pins, P/D, H/D, and W/D. As such, developing a correlation that accurately predicts the friction factor for all geometric parameters and over a wide range of Reynolds number, is a complex task.

Two main studies have been conducted to evaluate these correlations against the existing data sets by Bubelis and Schikorr in 2008 [10] and Chen Tondreas and Nguyen in 2013 [1]. Others have evaluated correlations to experimental data, but these two were the most comprehensive. Bubelis and Schikorr provided a qualitative evaluation based on visual inspection of the correlations and concluded the Rehme model offered the superior prediction. Cheng et al. provided a more quantitave evaluation based on three criteria, the prediction error distribution, and agreement index, and an assigned credit score. Their conclusion was the CTD correlation offered the best prediction.

For comparison to this data set, the four most relevant correlations were chosen based on the rankings from the two evaluations. Their ranges of applicability and uncertainties are shown in Table 3.

Table 3. Friction factor correlation applicability.

Correlation	# Pins	P/D	H/D	Re Range	Uncertainty
Cheng and Tondreas-D	19-217	1.0-1.42	4.0-52.0	$50\text{-}10^6$	±14%
Baxi and Dalle Donne	19-217	1.06-1.42	8.0-96.0	$50\text{-}10^5$	n/a
Kirillov	n/a	1.05-1.25	8.0-50.0	$50\text{-}2\text{x}10^5$	±15%
Rehme	7-217	1.06-1.42	8.0-50.0	$10^3\text{-}10^5$	±18%

The formulation of the CTD correlation used in this article accounts for the improvement in the transition flow regime described in a later publication [6]. The correlation proposed by Rehme has shown good agreement with experimental data in the turbulent regime, but its applicability cannot be extended to the laminar regime. The correlations proposed by Baxi and Dalle Donne (BDD) and Kirillov (KIR) are applicable to a wide range of Re number, but the transition from laminar regime and to turbulent regime are fixed (Re = 5000 and Re = 400 respectively) and independent of the bundle geometry. The BDD correlation is a combination of the Novenstern and Engel et al. correlations in the turbulent and transition and laminar regimes respectively. Because BDD comprises of both Novenstern and Engel, a direct comparison of the experimental data with these correlations is not performed.

6.2. Axial Pressure Drop

The primary method to evaluate the pressure response in this bundle was through a comparison of this work's bundle averaged friction factor with that of reference

correlations and existing data sets. The data set generated by the efforts presented includes a range of Reynolds numbers from Re 100 to Re 20,000 with two working fluids, DI water and p-Cymene.

Due to the destructive chemical reaction between p-Cymene and Acrylic, the bundle was rebuilt three times with each using different construction techniques. Although the geometry never differed between them and non-dimensionalising should allow for direct comparisons between working fluids, the data will be presented independently based on the bundle version and working fluid. Bundle 1 will be separated between water and p-Cymene. Bundle 2 and bundle 3 will also be separated, but only operated with p-Cymene as the fluid.

6.2.1. Bundle 1 – H_2O

Figure 5 shows a graph of the friction factor between PT4 and PT6, and PT5 and PT7 covering a Reynolds number from Re 3000 to Re 9500. In this configuration, it can be seen that the leading correlation, CTD, under predicts the friction factor compared to the experimental value.

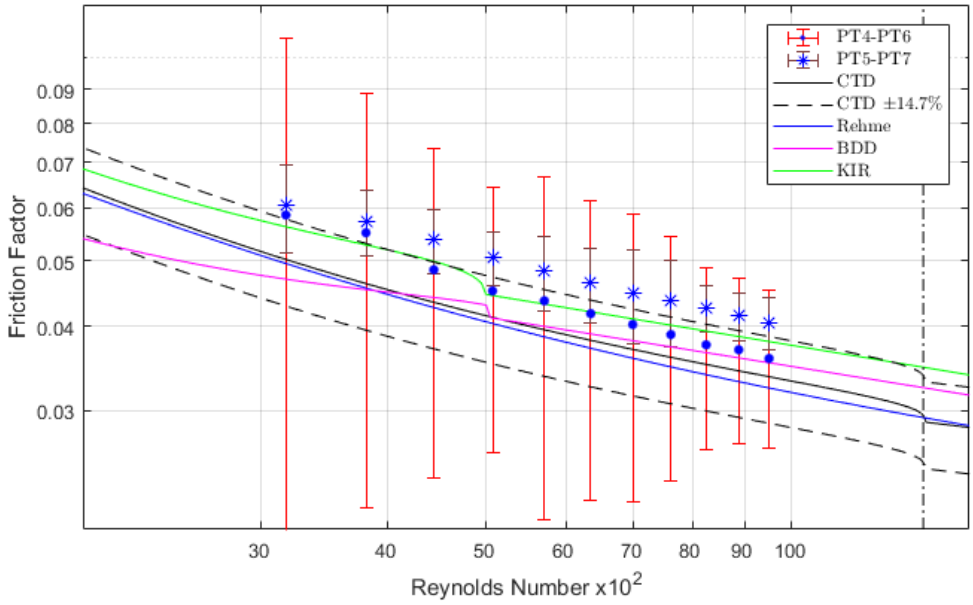

Figure 5. Bundle 1 water experimental friction factor

This result was not reproduced once the working fluid was changed to p-Cymene, and it was undesirable to fill the facility with water again for further investigation. The exact cause of this difference was never fully explored, but a few reasons were speculated to be the likely cause of this result.

Firstly, the friction factor was evaluated using the pressure drop between two gauge transducers attached to the framing of the facility hydraulically connected with tubing. Considering the measured pressure drop, excluding the change in elevation, is a very small number at low Re numbers, any deviation in elevation of the sensor compared to the pressure tap location introduces error into the measurement. The error bars also shown in the plot indicate that the predicted value lies within the uncertainty in the measurement.

6.2.2. Bundle 1 – p-Cymene

Figure 6 shows that the experimental friction factor decreased once the fluid was changed from water to p-Cymene. It is unknown why this shift occurred, but appears to be in excellent agreement with the CTD correlation. The elevation of the sensor can have an appreciable impact on the measured friction pressure drop and may be the cause of the shift.

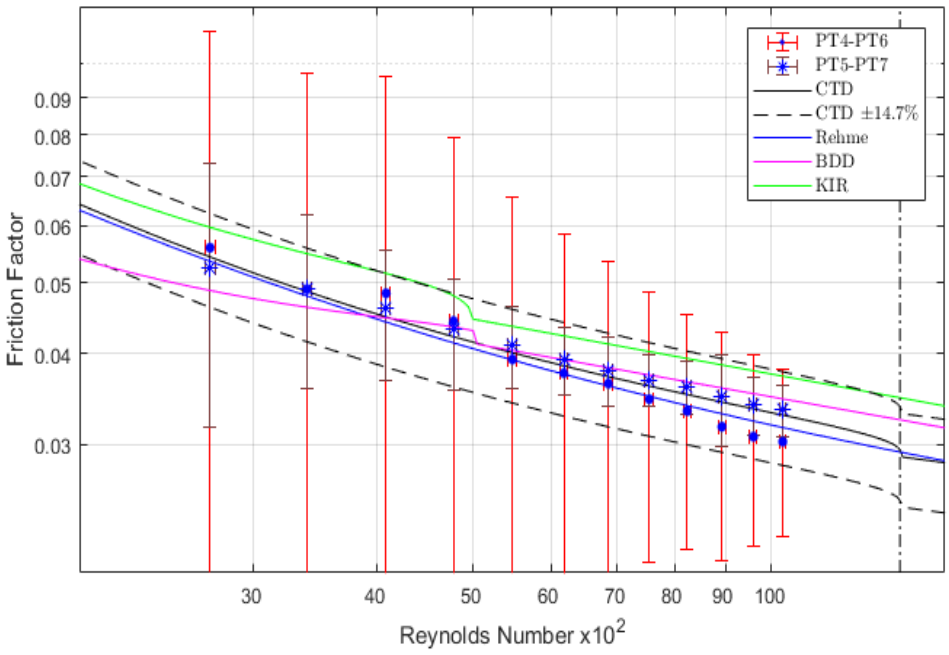

Figure 6. Bundle 1 p-Cymene experimental friction factor

6.2.3. Bundle 2 – p-Cymene

In efforts to minimize the measurement errors introduced by the sensor elevation, the sensors were attached directly to the duct wall. **Error! Reference source not found.** shows this disparity between the measurement between PT4 to PT6, and PT5 to PT7 remains. As Re number increases, there seems to be a deviation in the trend between the locations. The sensors between PT5 and PT7 were of a higher accuracy and deemed more reliable, and could explain the deviation in the trend between PT4 to PT6, and PT5 to PT7.

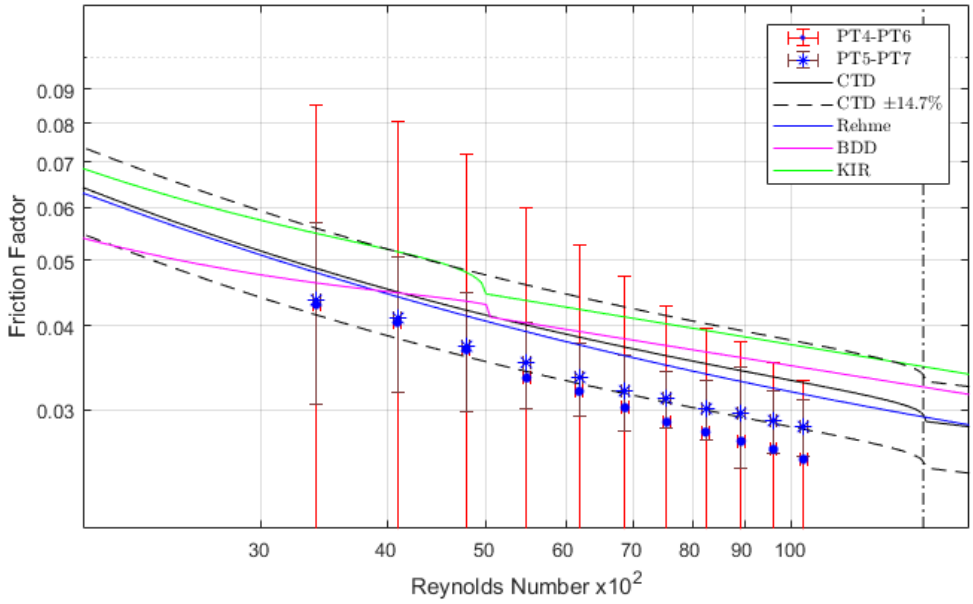

Figure 7. Bundle 2-pCymene: Experimental friction factor

All strain gauge sensors, which includes the pressure transducers used here, do not reproduce a completely linear output voltage with the applied pressure; the voltage

response at the extremes of the sensor's measurement range differs to the response in the middle of the sensor's range. The zero flow measurement, necessary to account for the hydrostatic head, results in a pressure measurement less than 5% of the transducers range between PT5 and PT7, and less than 1% between PT4 and PT6. The transducers between PT5 and PT7 are not only more accurate, but produce a more linear output. The higher accuracy and greater linearity between the sets of transducers could account for the deviatory behavior between the two measurement points.

Because the friction factor inversely related to the square of the velocity, the uncertainty in the calculation is higher at low Re numbers compared to higher Re numbers. It was evident that greater accuracy in the differential pressure measurement was required. To achieve this, a high accuracy differential pressure transducer was installed between PT 5 and PT 7.

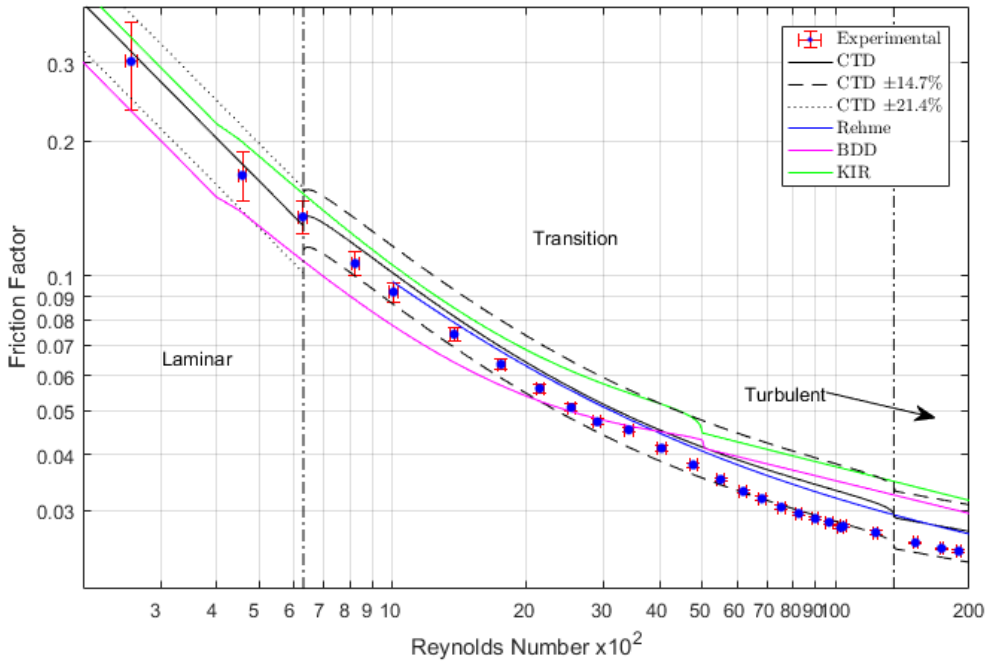

Figure 8. Bundle 2 p-Cymene: Experimental friction factor with axial DP

Figure 8 shows the result of utilizing the high accuracy DP on bundle 2 spanning a range in Re number, from about 250 to 20,000. The uncertainty is significantly diminished and a high degree of confidence in the reading is achieved. The experimental data matches very well in the laminar region, and is lower than the predicted value in the turbulent regime. This is postulated to be due to the acrylic rod's lower surface roughness compared to stainless steel, the material most other bundles were fabricated out of. The friction factor is not affected by surface roughness in laminar flows but is affected in turbulent flows.

The trend in the friction factor as a function of Re number can be described by Eq. 14, where f is the friction factor C_f is the frictional constant, Re is the Reynolds number, and m is the exponent that describes the trend.

$$f = \frac{C_f}{Re^m} \tag{14}$$

In the laminar region $m=1$. Figure 9 shows a zoomed picture in the laminar region, plotted is the experimental data points, the experimental laminar constant trendline, and the predicted trendline by the CTD correlation. The experimental laminar constant trendline was generated using a least squares regression and yielded a laminar constant $C_f=77.39$. The laminar constant predicted by CTD was $C_f=81.56$.

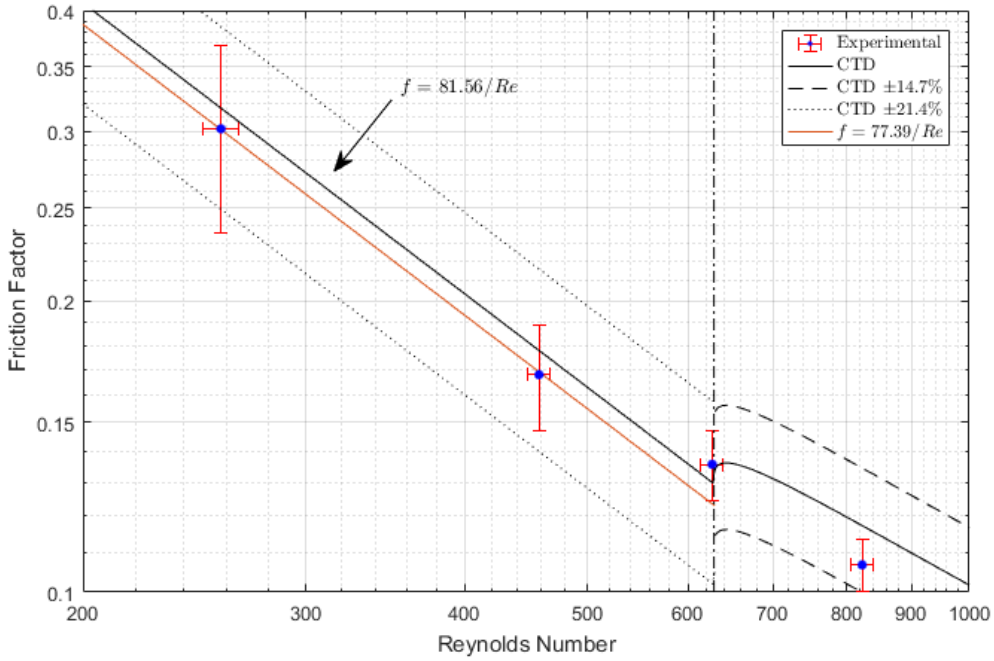

Figure 9. Bundle 2 p-Cymene: Laminar constant

The inflection at the laminar transition line is physical and has been demonstrated in other flow geometries such as smooth pipes [11]. This trend in the experimental data is visible and demonstrates that the prediction by CTD is reasonable at Re=627.

In the turbulent regime, the CTD correlation uses a value of *m=0.18*. This deviates from the value of *m=0.20* used for smooth pipe flow and could be contributed to surface roughness in the experimental data sets used by CTD.

Figure 10 shows a zoomed picture in the turbulent region; plotted is the experimental data points, the experimental turbulent constant trendline, and the predicted trendline by the CTD correlation. The experimental turbulent constant trendline was

generated using a least squares regression and yielded a turbulent constant C_f=*0.165,* and a value of *m=0.1945.* The turbulent constant predicted by CTD was C_f=*0.16.* This suggests that the with this geometry, the correlation accurately predicts the trend in the friction factor, but is shifted down, possibly because acrylic is smoother than stainless steel.

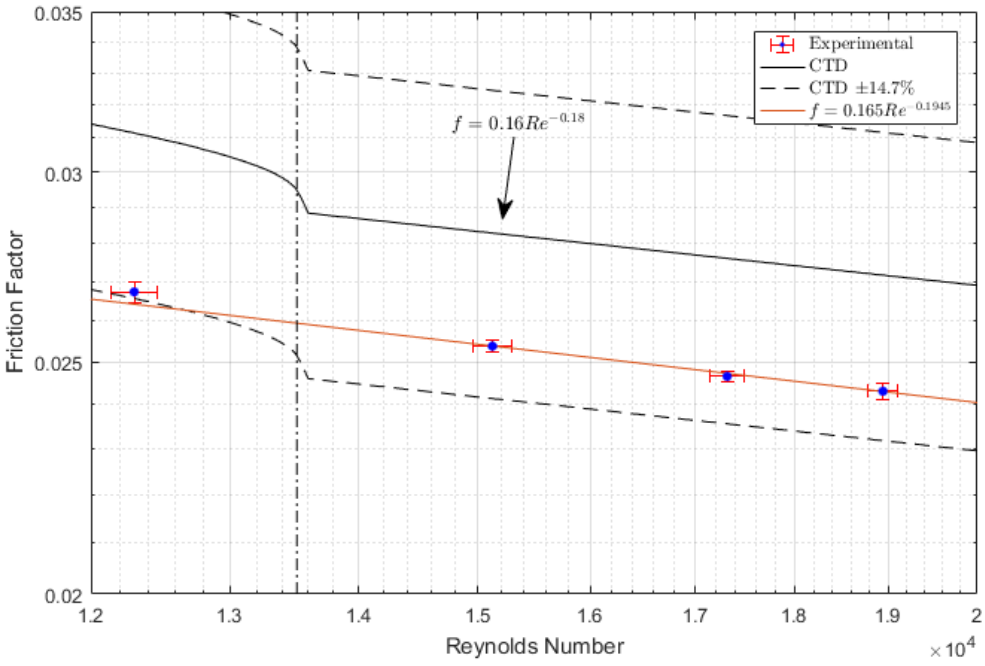

Figure 10. Bundle 2 p-Cymene: Turbulent constant

6.2.4. Bundle 3 p-Cymene

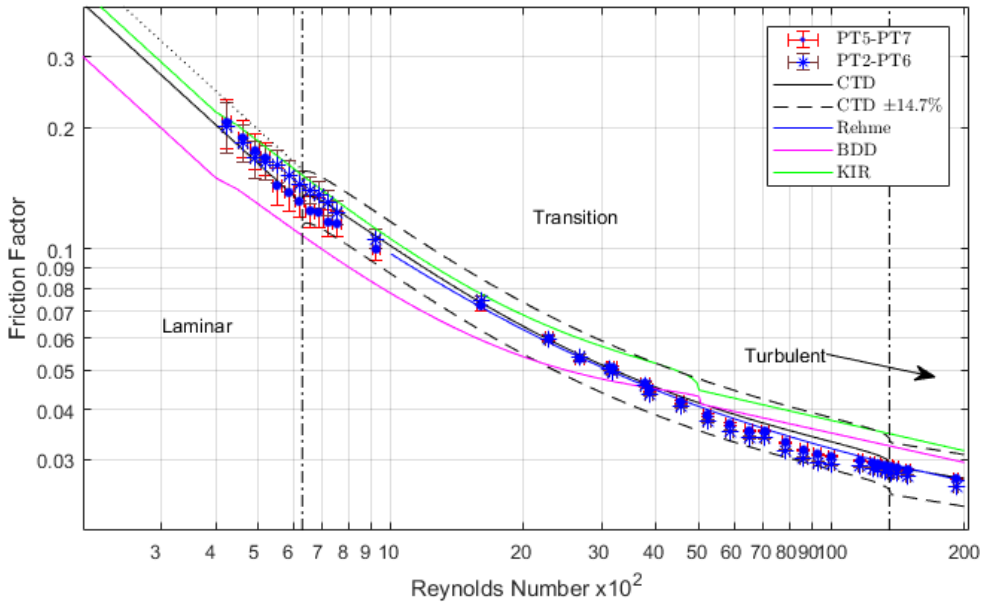

Figure 11. Bundle 3 p-Cymene: Experimental friction factor

Bundle 3 utilized a different technique in fabricating the rods and wires which resulted in an increase in the surface roughness compared to the previous bundles. Figure 11 shows the experimental friction factor as a function of Reynolds number for two locations, from PT5 to PT7, and from PT2 to PT6. The second location spans two wire pitches compared to one wire pitch between PT5 and PT7. The first four data points, from Re 425 to Re 550, are in very close agreement. At Re 550, PT2-PT6 the friction factor evaluated from PT5 to PT7 drops abruptly. Any deviation from linear behavior in the laminar regime indicates that some transition from laminar flow may have occurred. The two measurement locations do not follow the same behavior, PT2 to

PT6 remains slightly higher than PT5 to PT7 until the data crosses each other in the transition to turbulent regime. PT2 to PT6 then remains lower than PT5 to PT7 in the turbulent regime. The differential pressure transducer spanning two pitches is slightly less accurate than the one located between PT5-PT7, which could account for this deviation. At PT5 and PT7 the wire is at +30°, and at PT2 and PT6 the wire is at -60°, with respect to face F. It is expected that the same relative position for the measurement points should negate any wire effects of the pressure drop; the azimuthal pressure distribution should be the same at pitch elevations with the same wire angle. This expectation may not be correct and could be the cause of the deviatory behavior between the two measurement locations. PT2 is also closer to the inlet plenum, and entrance effects could impact the pressure drop as well.

Figure 12 shows a zoomed in region in the laminar regime. Bundle 3 yielded a laminar constant of 83.23. This is higher than bundle 2 and slightly higher than the correlation prediction. More data points were generated in the region where the transition from laminar conditions is expected. Unfortunately, there is some scatter in the data and it is difficult to draw hard conclusions. PT5 to PT7 displayed a sharp decrease at Re 550, but then returned to a linear trend. PT2 to PT6 also showed a deviation from linear behavior, but in the opposite direction as PT5 to PT7, then returned to a linear trend. It is likely the transition from laminar conditions is not as clear in this complex geometry compared to more simple geometries such as smooth pipes, and the total span of the wire pitch as well as the wire clock angle relative to the pressure tap could also have an impact.

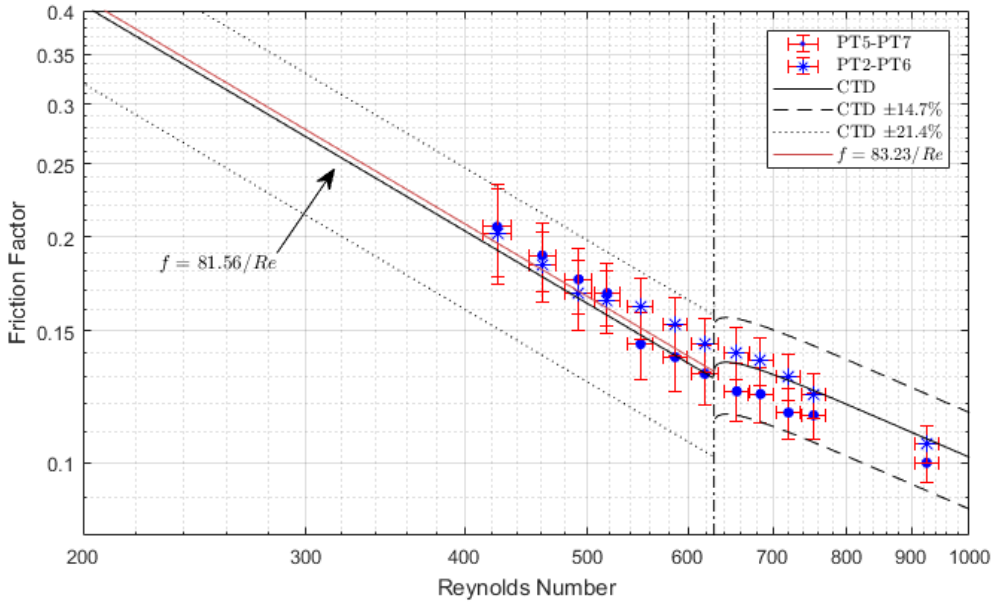

Figure 12. Bundle 3 laminar constant

Figure 13 shows a zoomed picture in the turbulent region for bundle 3; plotted is the experimental data points, the experimental turbulent constant trendline, and the predicted trendline by the CTD correlation. The trendline observed from PT5 to PT7 has a slightly different slope than the predicted trendline. PT2 to PT6 shows a lower friction factor that of PT5 to PT7, which is unexpected. Pressure tap 2 is located at wire axial pitch level 1.00, close to the lower plenum. It would be expected that the entrance effects near PT2 would increase frictional losses and cause the experimental friction between PT2 and PT6 to be larger than PT5 to PT7.

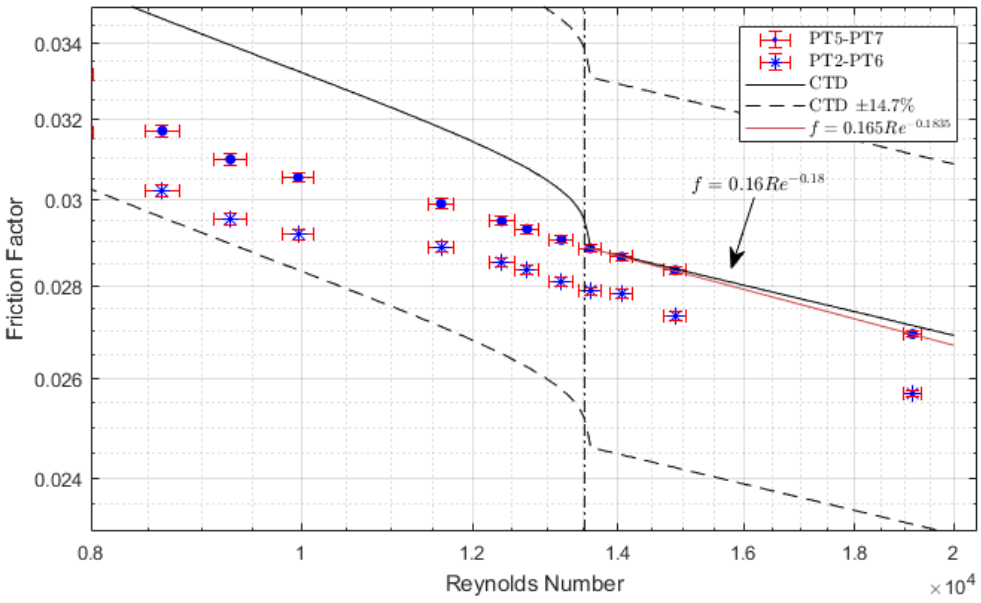

Figure 13. Bundle 3 turbulent constant

The inflection point at the turbulent transition line seen in the CTD prediction from transition to fully turbulent is not physical. It is caused by the equations used in the CTD formulation. The predicted transition point occurs at Re=13,500. Seen in Figure 13 are a few experimental data points that lie on the experimental turbulent trendline despite being in the transition regime. This suggest that this experimental bundle possibly transitions to turbulent flow before the predicted value.

6.2.5. Bundle Comparisons

Table 4. Bundle Timeline

Date	Bundle	Fluid	Transducer	Wire Method
Apr-16	Version 1	Water	Gauge	Top, Bottom
Apr-16	Version 1	p-Cymene	Gauge	Top, Bottom
Jun-16	Version 2	p-Cymene	Gauge	Entirety
Jun-16	Version 2	p-Cymene	DP	Entirety
May-17	Version 3	p-Cymene	DP	Dipped

Table 4 shows the progression of the test bundles. The first bundle was constructed with only the wires attached at the top and the bottom of the rod. This method will most likely be used in the commercial reactors where the wire is welded at the bottom of the fuel pin, wrapped around the pin, tensioned, and welded at the top. This was attempted for bundle 1, but the wires could not handle the stress induced by the flow and broke. The attachment process for bundle 2 was similar to bundle 1, with the exception that the wires were then glued along both sides for the entirety of the rod length. This bundle eventually too failed. The construction of bundle 3 involved fabricating similarly to bundle 2, then dipping the glued rod and wire with the wire into a tube filled with glue. It was hopeful that this technique would increase the longevity of the test bundle, but it also noticeably increased the surface roughness of the rods.

Figure 14 shows a comparison plot of bundle 3 and bundle 2. They are in close agreement in the laminar region, with bundle 3 being slightly higher, and continue to follow a similar trend into the transition region. Between Re 1000 and Re 2000, the friction factors begin to deviate with bundle 3 showing a higher friction factor. This continues through the turbulent regime. This is a good indication that the greater surface roughness of the rods and wires in bundle 3 causes an increase in friction factor. Friction factor is not affected by surface roughness in the laminar regime, but is in the turbulent regime. Cheng stated that not all subchannels transition at the same time; the subchannels in the interior transition first, and as Reynolds number increases, transition propagates radially. This slow divergence between bundle 3 and bundle 2, beginning after the transition from laminar and continuing into the turbulent regime, indicates that surface roughness could be the cause.

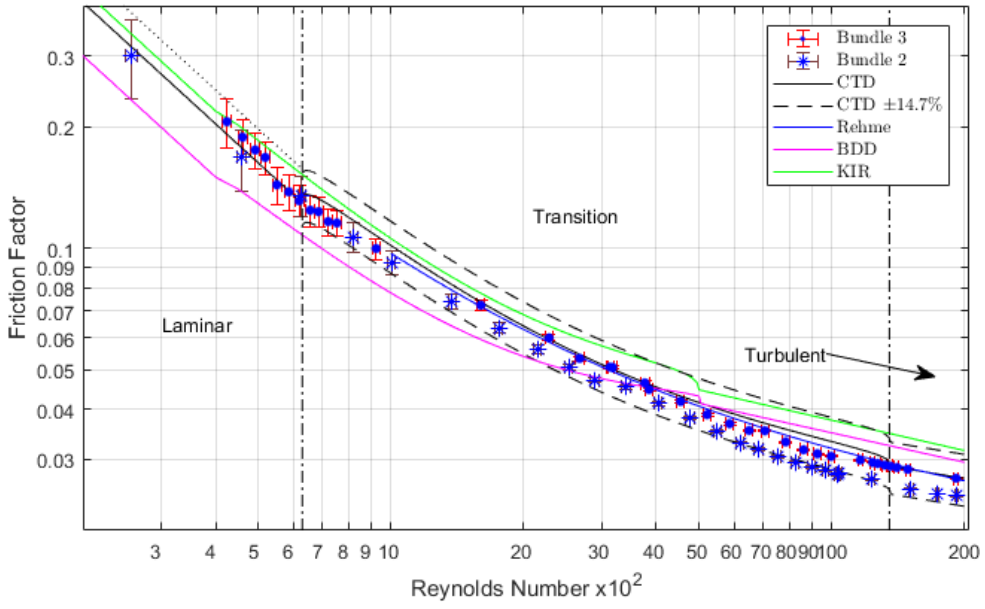

Figure 14. Comparison of bundle 3 to bundle 2

There appears to be an inflection point in the experimental trend for both bundles at approximately Re ~ 3400. As stated before, the experimental friction factor is estimated from Eq. 3, based exclusively on edge subchannel pressure drop and the bundle averaged Reynolds number. Cheng showed that for low Reynolds numbers (between 200–3000), the pressure drop in the edge subchannel is greater than the bundle-averaged pressure drop, and that for Re greater than 3000, the bundle-averaged pressure drop is greater than the edge subchannel pressure drop [12]. Subsequently, using the edge subchannel pressure drop to calculate the friction factor of the bundle would result in an experimental friction factor that is overvalued at Re $\lesssim$ 3000 and undervalued at Re $\gtrsim$ 3000. This is also the same point in which the friction factor estimated from PT2-PT6 crosses over the estimate from PT5-PT7 as shown in Figure 11.

6.3. Azimuthal Pressure Drop

Azimuthal pressure drop data was taken at two axial locations. Figures Figure 15 andFigure 16 show the azimuthal change in pressure with respect to face F from Re 250 to Re 20000 at locations PT5 and PT6 respectively. The right side of the figures show the location of the wire clock angle. At the PT5 and PT6 axial location, four of the faces contain a pressure tap referred to as face A, D, E, and F. A differential pressure transducer was used to measure the change in pressure between the faces with one side permanently fixed to face F. As such, each measurement is in reference to face F.

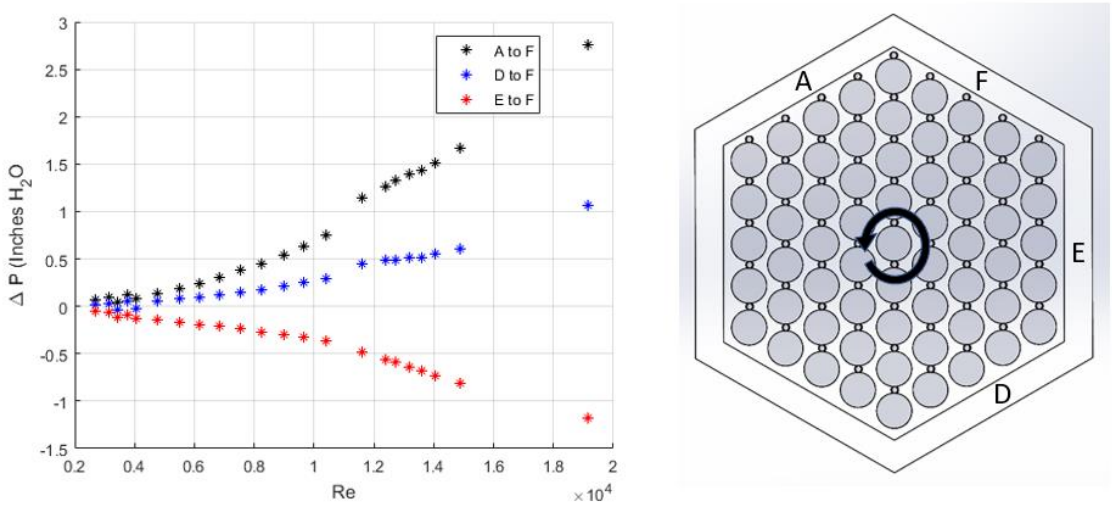

Figure 15. Azimuthal pressure drop at PT5

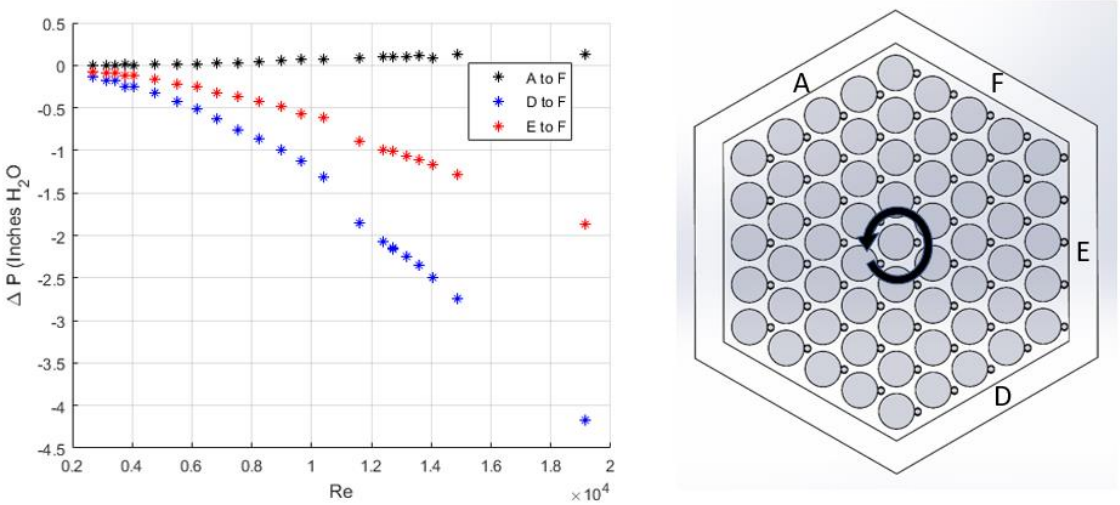

Figure 16. Azimuthal pressure drop at PT6

The general trend for the azimuthal pressure drop is for there to be a pressure gradient perpendicular to the wire. If the wire is at the 12:00 position, the gradient will propagate from the 3:00 position to the 6:00 position. The direction of the gradient is dependent on the direction the wire is rotating; the high pressure side is the side the wire is turning towards, and the low pressure side is the side the wire is turning away from. This behavior is the greatest contributor to the transverse pressure drop, but some CFD simulations show secondary contributor [13]. If the wire is said to be due north with respect to the rod, the subchannels directly south will show a higher pressure, but the effect is minimal compared to the pressure gradient east and west.

The behaviors described above are clearly replicated in the plots of this experimental data. Because the wire is rotating counter-clock-wise, at PT5 the pressure gradient should be lowest at face E, and highest directly across from it, face B. The plotted values are with respect to face F, and it can be seen that face A is higher than face E. The other “North and South” trend is also visible as face D is greater than face F.

At PT6 the maximum pressure would be expected in the corner between face F and face A, and the minimum pressure between face D and face C. Face E is greater than face D and face F is greater than face E. Both face F and face A are equidistant to the expected location of maximum pressure and is the reason the change in pressure from A to F is minimal, but A is slightly greater than F which is the expected result. It was not possible to perform a quantitative evaluation of the transverse pressure gradient, but as shown in this section, a qualitative analysis shows the validity of these results.

7. CHALLENGES AND IMPROVEMENTS

As shown in the previous section, instrument accuracy and having the correct instrument for the parameter of interest can greatly improve results. The initial use of gauge pressure transducers to evaluate the friction factor was a mistake. They introduced potential error when they were not attached to the duct wall. The accuracy of the instrument also needs to be taken into consideration. Minimal conclusions can be drawn from data if the uncertainty in calculated variables, such as the bundle averaged friction factor, is too great. The frictional pressure drop ranged from less than 20 Pa at Re 500 to 3500 Pa at Re 19000. The full scale pressure on the initial transducers is 200,600 Pa. The measured value of the parameter of interest needs to be on the same order of magnitude as the capability of the instrument. It is also important to consider unavoidable limitations of instruments such as the non-linearity of strain gauges. This non-linearity can introduce further error if the parameter of interest is calculated based on measurements that lie on the extremities of the instruments capabilities. The higher accuracy gauge transducers placed between PT5 and PT7 produced results that were in agreement with the high accuracy differential transducer, but the propagated uncertainty was still larger than desired.

It was known at the beginning of the project that the working fluid would change from water to p-Cymene. Given that turbine flow meters are impacted by both density and viscosity, the meter's calibration will not be the same between different fluids. The use of differential pressure flow meters, such as orifice plates, was disallowed because

they required too long of straight pipe runs than the limited space would allow, and decreasing the pipe diameter would have increased the pumping requirements. It was possible to use the pitot tube because the test section was bypassed, and the pipe diameter could be decreased. A vortex shedding flowmeter could have alleviated these issues and allowed for the fluid to be switched without requiring additional calibration.

Care was taken with the pressure transducers to make sure they were operating correctly before each test. This was not the case with the flow meter. The flow meter was rated to remain in calibration with minimal drift for a period of 5 years. Thus, it was assumed that after the in house calibration, the rotation of the turbine as a function of volumetric flow rate would remain constant for that period of time. Some time had passed during the decommission of bundle 2 and the construction of bundle 3, and it was found that the calibration had changed. This was verified by performing the calibration with the pitot tube again. It is speculated that some material incompatibility with the turbine bearings and p-Cymene caused the shift. With reliance on a single instrument for the volumetric flow rate, it was difficult to verify the flow meter was metering correctly; the bypass loop and test section were not installed simultaneously. A different approach to this verification is to check against a physical or known trend. The friction factor should always follow the trend of Eq. 14, and by plotting this trend as a function of Reynolds number as shown in the results section, a deviation indicates that some measured value is not correct.

One limitation in the methodology used in this work is the location of the pressure taps. With the instrument being located only on one face, the measured pressure

drop is representative of the edge subchannel and not the pressure drop through the entire bundle. The Reynolds number produced was derived from the volumetric flow rate and is representative of the bundle averaged Reynolds number. Chen performed experiments that showed the axial fluid velocity is not the same in all subchannels. Thus, there exists some deviation in subchannel Reynolds number and the bundle averaged Reynolds number [12]. Marten et al. showed that the error in the evaluated friction factor induced by using the bundle averaged Reynolds number with the pressure drop in the edge subchannel is on the order of 2% [14]. One way to avoid this error is to hydraulically link the pressure taps on each of the six faces, at both axial elevations, and measure the pressure drop between these unions. This counteracts the wire effect and allows for a bundle averaged pressure drop measurement. It was also shown that the wire clock angle did not impact the evaluated friction factor, so the effect of connecting all faces seems to be that it averages and negates the wire effects.

8. FUTURE WORK

Suh proposed a model to estimate the azimuthal pressure drop [15]. Essentially the model discretizes the wire into axial segments and approximates the discretized wire segments as vertical with a corresponding wire clock angle. The pressure drop azimuthally is estimated by assuming the behavior of the transverse velocity component is similar to the behavior of crossflow in rod banks with wires attached. Also assumed is that because flow is primarily axial through a nuclear rod bundle, “entrance” effects are small and can be neglected. Thus, fully developed crossflow is applied to the tangential velocity to derive an empirical estimation for azimuthal pressure drop. To apply this model, knowledge of the tangential velocity is required. One of the model limitations is that it cannot account for the case where the wire is at the 90° clock location. There is no data available for transverse rods in this configuration because the wires would completely block the subchannel and no flow would occur.

So far, this work has only produced pressure measurements on the wall of the duct, the edge subchannel. Instrumented rods would allow for the quantification of the pressure drop in the interior subchannels. The CTD correlation is the only correlation that predicts the pressure drop on a subchannel basis. Instrumented rods and accurate velocity data from PIV measurements would allow for the evaluation of the performance of existing correlations and models.

One of the reasons the transition region is difficult to predict is that not all subchannels undergo the transition from laminar at the same time. Cheng states that the

interior subchannels undergo this transition first, so the bundle transition region, as stated in this work and other literature, is really a combination of subchannels in different flow regimes [12]. It is possible instrumented rods in various locations could aid in describing which undergo the transition first and the propagation of that behavior.

Current correlations are only valid for one wire spacer lead length. No correlation exists that accounts for how the pressure drop changes as a function of wire clock angle. Existing subchannel analysis codes distribute the predicted value over an entire spacer length evenly when discretizing the domain. Instrumented pressure rods with pressure taps along multiple locations within a wire spacer lead length could resolve how this pressure drop is distributed in reality. Though CFD is becoming more and more prominent, analysis for long term transient events, such as accident analysis, will likely rely on subchannel codes. Improvement in the models that subchannel codes utilize will increase their effectiveness to accurately predict thermal-hydraulic behaviors.

The fluctuating component of pressure is more difficult to accurately measure compared to static pressure. Current imaging techniques allow for the instantaneous velocity measurements, and when coupled with instantaneous pressure measurements, it is possible to reconstruct the entirety of the pressure field. This would be very beneficial when used to validate CFD models.

9. CONCLUSIONS

This work has produced a data set for both the axial and azimuthal pressure drop in a 61-Pin hexagonal wire-wrapped fuel bundle. A qualitative analysis of the azimuthal pressure drop is presented in this work. The experimental friction factor was evaluated and for broad range of Reynolds number, form 200-20,000, and the uncertainty was quantified. The results were plotted against relevant friction factor correlations where CTD and Rehme were found to be the most accurate in the transition and turbulent regime. CTD not only accurately predicted friction factor in the turbulent regime, but also fit the data very well in the laminar regime. Three bundles were fabricated with the same geometric parameters, but with different approaches for attaching the wires to the rods. The friction factor was not the same between all three bundles. Bundle 3 produced a higher bundle averaged friction factor in the turbulent regime and matched in the laminar regime. The primary difference between bundle 3 and the others was the measurable difference in the surface roughness caused by the fabrication technique. Considering surface roughness impacts turbulent flows but not laminar flows, the data presented in this work suggests the higher friction factor for bundle 3 was caused by the increase in surface roughness.

REFERENCES

[1] Cheng, S.K., Tondreas, N.E., and Nguyen, N.T., 2014, "Evaluation of Existing Correlations for the Prediction of Pressure Drop in Wire-Wrapped Hexagonal Array Pin Bundles," *Nucl. Eng. Des.,* no. 267, pp. 109-131.

[2] Novendstern, E., 1972, "Turbulent Flow Pressure Drop Model for Fuel Rod Assemblies Utilizing a Helical Wire-Wrap Spacer System," *Nuc. Eng. Des.,* no. 22(1), pp. 19-27.

[3] Rehme, K., 1967, *Geometry-Dependence of the Pressure Loss in Rod Bundles With Coiled Wire Spacers and Longitudinal Flow,* Ph.D. dissertation, Karlsruhe Institute of Technology, Karlsruhe, Germany.

[4] Engel, F., Markley, R., and Bishop, A., 1979, "Laminar, Transition and Turbulent Parallel Flow Pressure Drop Across Wire-Wrap-Spaced Rod Bundles," *Nucl. Sci. Eng.,* no. 69(2), pp. 290-296.

[5] Cheng, S. K., and Tondreas, N. E., 1986, "Hydrodynamic Models and Correlations for Bare and Wire-Wrapped Hexagonal Rod Bundles-Bundle Friction Factors, Subchannel Friction Factors and Mixing Parameters," *Nuc. Eng. Des.,* no. 92(2), pp. 227-251.

[6] Chen, S. K., Petroski, R., and Tondreas, N. E., 2013, "Numerical Implementation of the Cheng and Tondreas Correlation for Wire Wrapped Bundle Friction Factors-

Desirable Improvements in the Transition Flow Regimes," *Nucl. Eng. Des.*, no. 263, pp. 406-410.

[7] Baxi, C. B., and Dalle Donne, M., 1981, "Helium Cooled Systems, the Gas Cooled Fast Breeder Reactor," Pergamon Press, Elmsford, NY, pp. 410-462.

[8] Kirillov, P. L., Petroski, Bobkov, V. P., Zhukov, A. V., and Yuriev, Y. S., 2010, "Handbook on Thermohydraulic Calculations in Nuclear Engineering," in *Thermohydraulic Processes in Nuclear Power Facilities*, Vol. 1, Energoatomizdat, Moscow, Russia.

[9] Cameo Chemicals, 1999, "p-Cymene Chemical Information Sheet," Silver Spring, MD, accessed Oct. 10, 2017, https://cameochemicals.noaa.gov/chris/CMP.pdf

[10] Bubelis, E., and Schikorr, M., 2008, "Review and Proposal for Best Fit of Wire-Wrapped Fuel Bundle Friction Factor and Pressure Drop Predictions Using Various Existing Correlations," *Nucl. Eng. Des.*, *238*, pp. 3299-3320.

[11] Munson, B. R., Rothmayer, A. P., Okiishi, T. H., and Huebsch, W. W., Fundamentals of Fluid Mechanics, New Jersey: Wiley, 2012.

[12] Cheng, S. K., 1986, *Constitutive Correlations for Wire-Wrapped Sub-Channel Analysis Under Forced and Mixed Convection Conditions*, Ph.D. dissertation, Massachusetts Institute of Technology, Cambridge, Massachusetts.

[13] Jeong, J. H., Yoo, J., Lee, K.L., and Ha, K. S., 2015, "Investigation Of Wire Effect in a Wire-Wrapped 37-Pin Fuel Assembly," in *ASME-JSME-KSME Joint Fluids Engineering Conference*, Seol, Korea.

[14] Marten, K., Yonekawa, S., and Hoffman, H., 1987, "Experiments and Correlation of Pressure Loss Coefficients for Hexagonal Arranged Rod Bundles (P/D > 102) With Helical Wire Spacers in Laminar and Turbulent Flows," KFK--4038, Karlsruhe, Germany.

[15] Suh, K. Y. Tondreas, N. E., 1986, "An Experimental Correlation of Cross-Flow Pressure Drop for Triangular Array Wire-Wrapped Rod Assemblies," *Nucl. Tech.*, vol. 76(2), pp. 229-240.

APPENDIX A

$$A_1 = \left(\frac{\sqrt{3}}{4}\right)P^2 - \frac{\pi D^2}{8} - \frac{\pi D_w^2}{8\cos(\theta)}$$

$$A_2 = \left(W - \frac{D}{2}\right)P - \frac{\pi D^2}{8} - \frac{\pi D_w^2}{8\cos(\theta)}$$

$$A_3 = \frac{\left(W - \frac{D}{2}\right)^2}{\sqrt{3}} - \frac{\pi D^2}{24} - \frac{\pi D_w^2}{24\cos(\theta)}$$

$$A_{Bundle} = N_1 A_1 + N_2 A_2 + N_3 A_3$$

$$P_{wet,1} = \frac{\pi D}{2} + \frac{\pi D_w}{2\cos(\theta)}$$

$$P_{wet,2} = P + \frac{\pi D}{2} + \frac{\pi D_w}{2\cos(\theta)}$$

$$P_{wet,3} = \frac{\pi D}{6} + \frac{2\left(W - \frac{D}{2}\right)}{\sqrt{3}} + \frac{\pi D_w}{6\cos(\theta)}$$

$$P_{wet,Bundle} = N_1 P_{wet,1} + N_2 P_{wet,2} + N_3 P_{wet,3}$$

$$\cos(\theta) = \frac{H}{\sqrt{H^2 + \left(\pi(D + D_w)\right)^2}}$$